

Article

A Tangent Release Manipulation Controlled by a Dual-Arm Space Robot

Xiaoyi Wang ^{1,*}  and Jayantha Katupitiya ²

¹ School of Electrical Engineering and Telecommunications, University of New South Wales, Sydney, NSW 2052, Australia

² School of Mechanical and Manufacturing Engineering, University of New South Wales, Sydney, NSW 2052, Australia; j.katupitiya@unsw.edu.au

* Correspondence: xiaoyi.wang@unsw.edu.au

Abstract: As people further develop space with advanced technology, space robots have played a significant role in on-orbit servicing missions. Space robots can carry out more risky and complicated missions with less cost than astronauts. Dual-arm space robots can perform complex on-orbit space missions more effectively than single-arm space robots. Since the coupled dynamics between the free-floating base and the arms exist in space robots, accurate coordinate control of the base and the arms is essential. Spacecraft release missions have been proposed to berth/deberth a spacecraft to a space station. Based on the existing release missions, a tangent release strategy is introduced in this paper, which can release a space object in the tangent direction of the final link of a space manipulator. This strategy can control a dual-arm space robot to deploy cargo/spacecraft in variable directions in 3D space without thrusters and the associated fuel consumption. For instance, this tangent release operation can transport cargo or modules of large-scale spacecraft needing on-orbit assembly. Considering model uncertainties, robust controllers against model uncertainties that are used to control the dual-arm space robot with high accuracy. Hence, a robust sliding mode controller (SMC) is utilized to accurately control the space robot to carry out the proposed tangent release strategy. For comparison, we select a conventional computed torque control (CTC) implemented by a PD-type controller. In the simulations, the SMC performs better in tracking accuracy and robustness against the model uncertainties than the PD controller. Numerical simulations indicate the feasibility and effectiveness of the tangent release manipulation of a space object by a dual-arm space robot.

Keywords: space robot; dual-arm space robot; coordinated motion control of space robots; sliding mode control; spacecraft release strategy



Citation: Wang, X.; Katupitiya, J. A Tangent Release Manipulation Controlled by a Dual-Arm Space Robot. *Actuators* **2023**, *12*, 325. <https://doi.org/10.3390/act12080325>

Academic Editors: Dengqing Cao, Xiangying Guo and Shuai Chen

Received: 11 July 2023

Revised: 8 August 2023

Accepted: 13 August 2023

Published: 14 August 2023



Copyright: © 2023 by the authors. Licensee MDPI, Basel, Switzerland. This article is an open access article distributed under the terms and conditions of the Creative Commons Attribution (CC BY) license (<https://creativecommons.org/licenses/by/4.0/>).

1. Introduction

On-orbit space robots with robotic manipulators play a critical role in assembling, repairing, refueling, and transporting operations in space [1,2]. A space robot system for on-orbit servicing operations consists of three major components: the base, one or multiple space manipulators, and the object to be serviced [2]. A typical capture process of a space object by a space robot incorporates four phases: observation, approach, capture, and postcapture [2]. Due to the microgravity environment of space, the coupled dynamics between the free-floating base and the arms exist. In other words, the base will simultaneously move when its attached space manipulator moves for an on-orbit servicing mission. Thus, researchers investigate the strategies to simultaneously control the base and the manipulators to carry out the complex space missions [3–7].

Space manipulators can also be used to deploy, release, and retrieve spacecraft [2]. For instance, operations to redock modules on the MIR orbital station were developed in [8]. This operation could effectively transfer a module of the MIR orbital station from one side to another side port, which included a release operation and a redocking operation [8].

Hence, release operations in three-dimensional (3D) space can help transfer space objects like modules or cargo for spacecraft. Unlike just radially pushing the object away along the directions of the final link, the tangent release can flexibly transfer the object in variable directions to locations in the neighborhood of the space robot without using thrusters. However, a strategy to release the object at a desired velocity tangent to the final link (in a direction perpendicular to the final link) of the space robot is worthy of being investigated. Additionally, dual-arm space robots can perform complex on-orbit space missions more effectively than single-arm space robots [9], which may be suitable for complex tangent release manipulation.

Typically, on-orbit capture operations carried out by free-floating space robots can only grasp and move the space object in the workspace of the space robot [10,11]. Moreover, the trajectories of the end-effectors need to be carefully designed to avoid singularity configurations during the on-orbit operations by the dual-arm space robots [12]. Thus, the workspace of the space robot needs to be extended for easier on-orbit assembly or short transportation of cargo between spacecraft. A tangent release strategy of a space object by a free-floating space robot can fulfil the requirements of transporting a space object at a desired tangent velocity without the need for the fuel of thrusters. Compared with single-arm space robots, dual-arm space robots can carry out more complicated tasks like capturing tumbling targets with a higher probability of success [13,14]. Compared with the mission to grasp an object and move it by a space robot, the tangent release strategy may transfer the object to more variable directions. Therefore, research on dual-arm space robots has great significance in on-orbit serving missions.

Since complex on-orbit missions need to be accurately carried out, controllers with good robustness and high accuracy need to be developed for dual-arm space robots [15–17]. Jia and Misra [18] presented a robust adaptive sliding mode controller to make a dual-arm space robot follow the desired trajectories. As model uncertainties of the inertial parameters of dual-arm space robots may exist in the complex space environment, a dynamic-based adaptive control method was proposed to be applied to a dual-arm space robot [19]. Moreover, optimal control was developed for dual-arm space robots to reduce the energy consumption of an on-orbit mission [20]. Therefore, control methods should be compared and carefully selected for complex space operations carried out by dual-arm space robots.

Considering the complex environment in space, model uncertainties in mass or inertial parameters may exist in a space robot system, which can influence the robustness performance of controllers. Conventional feedback PID controllers have been utilized to control space manipulators [21]. However, PID controllers cannot stabilize nonlinear systems with model uncertainties [22]. Therefore, control methods with better robust performance will be developed to control the dual-arm space robot. Many control methods, such as sliding mode control [15], neural network control [23], optimal control [7,24,25], and adaptive control [26,27], were utilized to control space robots and spacecraft. Considering the robustness against model uncertainties, sliding mode control (SMC) with good robustness is selected to control the dual-arm space robot. Even though references [15,26] used SMC to control spacecraft with uncertainties, they only applied one set of uncertain parameters to the space robot in their numerical simulations. To analyze the robust performance of a controller for practical applications, a range of the uncertain physical parameters of a space robot should be compared in the simulations. Due to frequent switches of the signum function in the control law generated by the conventional SMC, there will be fluctuations in the control torques, which can be found in [15]. Thus, we develop a boundary layer method [28] to reduce the fluctuations in the control torques caused by the SMC.

Thus, this paper proposes a new tangent release strategy for a space object in 3D space by a dual-arm space robot. Compared with some release operations to directly push an object away, the proposed tangent release operation can release along an arbitrary direction within the appropriate task space of the space robot to transport cargo or modules of large-scale spacecraft needing on-orbit assembly. For instance, the potential tangent release operation can effectively transfer a module of a space station from one side to

to make the space robot and the space object rigidly connected as a combined system during the pick-up phase. For instance, the space object can be considered the cargo picked up by the two manipulators in the cargo bay. During the pick-up phase, the combined system gradually rotates around its center of mass (CM) with respect to the inertial frame. When the desired angular velocity of the combined system is obtained, the space robot will release the space object and smoothly move to a stand-by configuration during the postrelease phase.

The advantage of the tangent release strategy is that the space object can obtain a desired velocity tangent to the final links of the space robot when the end-effectors release the object. Usually, space robots release a space object in a radial direction to push the space object away. To expand the releasing directions by space robot, the tangent release strategy is investigated. Moreover, the release strategy can release the space object in an arbitrary safe direction, which can be useful to carry out future space missions such as transporting cargo between spacecraft and redocking modules of a spacecraft for assembly and maintenance.

2.1. Assumptions

Figure 2 demonstrates the model of the space robot to tangentially release a space object in space.

- Σ_B Base Frame
- Σ_G Space Robot Frame
- Σ_I Inertial Frame
- $\Sigma L_i^{(k)}$ Link Frame
- Σ_{SO} Space Object Frame
- Σ_C Combined System Frame
- Black points • Center of Mass (CM)

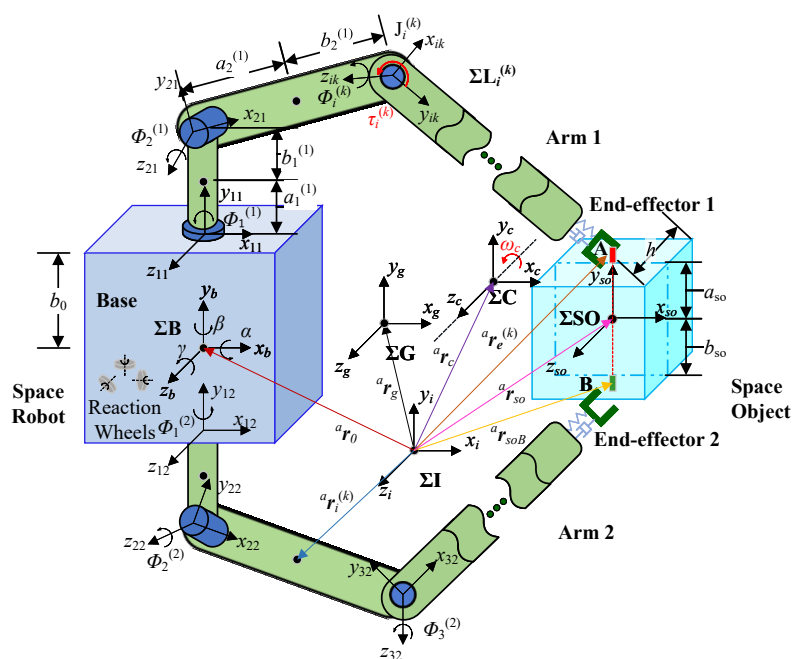


Figure 2. Dynamic model of a dual-arm space robot for a tangent release manipulation.

Some assumptions are made as follows.

1. According to Figure 2, the dual-arm space robot incorporates a rigid base and two rigid symmetrical arms. Each manipulator has n links with n degrees of freedom.
2. The orbital mechanics are ignored during the tangent release operation.
3. An initial configuration is set up to keep from singular configurations of the manipulators during the tangent release manipulation.

4. The space object is assumed as a rigid cuboid with an initial stationary status. The dual-arm space robot can grasp the two symmetric grasp points (A and B) of the space object and subsequently release the space object at a desired velocity.
5. The thrusters will not be ignited during the operation due to the impulse caused by the ignition. Reaction wheels (RWs) can regulate the base attitude of the space robot by exchanging angular momentum with the base.
6. There are negligible external forces or torques applied to the combined system, incorporating the space robot and the space object during the operation.
7. Geometrical parameters and the motion of the space object can be observed and precisely estimated by sensors of the space robot before the operation.

An explanation to Assumption 2: the tangent release operation is carried out in a quite shorter time (about 80 s in the simulations) than the orbital period of the space robot (approximately 90 min for low Earth orbit). Thus, we assumed that orbital mechanics can be neglected during the tangent manipulation.

2.2. Coordinate Systems

According to Figure 2, the coordinate systems in this paper are defined as follows: the inertial frame ΣI , the base frame ΣB , the space robot frame ΣG , Link $i^{(k)}$ frame $\Sigma L_i^{(k)}$, the space object frame ΣSO fixed in the CM of the object, and frame ΣC of the combined system of the space robot and the space object. The superscripts $^a\{\cdot\}$, $^0\{\cdot\}$, $^{i^{(k)}}\{\cdot\}$, $^{so}\{\cdot\}$, and $^c\{\cdot\}$ represent the variables in ΣI , ΣB , $\Sigma L_i^{(k)}$, ΣSO , and ΣC , respectively. When some variables do not show their superscripts, those variables will be denoted in the inertial frame.

2.3. Nomenclature

The symbols in Figure 2 are defined as follows:

$L_i^{(k)}$	the i -th link of k -th arm, $i = 1, 2, \dots, n, k = 1, 2$.
$J_i^{(k)}$	the i -th joint of k -th arm, $i = 1, 2, \dots, n, k = 1, 2$.
$^a r_g \in \mathbb{R}^3$	position vector for the center of mass (CM) of the space robot in ΣI .
$^a r_0 \in \mathbb{R}^3$	position vector for the CM of the base of the space robot.
$^a r_i^{(k)} \in \mathbb{R}^3$	position vector for the CM of $L_i^{(k)}$.
$^a r_e^{(k)} \in \mathbb{R}^3$	position vector for the CM of the k -th end-effector.
$^a r_{so} \in \mathbb{R}^3$	position vector for the CM of the space object (also set as the origin of ΣSO).
$^{so} r_{soA} \in \mathbb{R}^3$	position vector for grasp point A of the space object in ΣSO .
$^{so} r_{soB} \in \mathbb{R}^3$	position vector for grasp point b of the space object in ΣSO .
$^a r_c \in \mathbb{R}^3$	position vector for the CM of the combined system ΣC .
$b_0^{(k)} \in \mathbb{R}^3$	position vector from CM of the base to Joint $J_1^{(k)}$.
$a_i^{(k)} \in \mathbb{R}^1$	length from $J_i^{(k)}$ to CM of $L_i^{(k)}$.
$b_i^{(k)} \in \mathbb{R}^1$	length and from CM of $L_i^{(k)}$ to $J_{i+1}^{(k)}$.
$a_{so} \in \mathbb{R}^1$	length from CM of the space object to grasp point A.
$b_{so} \in \mathbb{R}^1$	length from CM of the space object to grasp point B.
$h \in \mathbb{R}^1$	height of the space object.
$\phi_s = (\alpha, \beta, \gamma)^T \in \mathbb{R}^3$	attitude vector of the base with respect to the inertial frame.
$m_0, m_i^{(k)}, m_{so} \in \mathbb{R}^1$	mass of the base, Joint $L_i^{(k)}$, and the space object, respectively.
$^a \omega_c \in \mathbb{R}^3$	angular velocity of the combined system with respect to the inertial frame.
$^a \theta_c \in \mathbb{R}^3$	rotational angle vector of the combined system with respect to the inertial frame.
$\tau_i^{(k)}$	the control torque applied to the i -th joint of k -th arm, $i = 1, 2, \dots, n, k = 1, 2$.
$\tau_b = (\tau_{bx}, \tau_{by}, \tau_{bz})^T$	the control torques from the three RWs to regulate the base attitude.

2.4. Space Robot Model

Based on our previous work [17,29–31], the Jacobian equation describing kinematics of a dual-arm space robot can be shown as

$$\dot{X} = J\dot{\phi} \tag{1}$$

where the vector $X = [\alpha, \beta, \gamma, r_{ex}^{(1)}, r_{ey}^{(1)}, r_{ez}^{(1)}, r_{ex}^{(2)}, r_{ey}^{(2)}, r_{ez}^{(2)}]^T \in \mathbb{R}^9$ represents the base attitude and the movement of the dual-arm space robot in the 3D task space. Vector $\phi = [\alpha, \beta, \gamma, \phi_1^{(1)}, \phi_2^{(1)}, \phi_3^{(1)}, \phi_1^{(2)}, \phi_2^{(2)}, \phi_3^{(2)}]^T \in \mathbb{R}^9$ describes the movement of the dual-arm space robot in the joint space. Matrix $J \in \mathbb{R}^{9 \times 9}$ is the Jacobian matrix.

To describe the base attitude and motion of end-effectors in 3D space, we select those nine elements for the state vector X . In addition, the size of the vector ϕ is selected as nine (same as X) to keep the possibility of the invertibility of the Jacobian matrix J .

In detail, $\phi_s = [\alpha, \beta, \gamma]^T$ represents the base attitude around x, y, z axes for the inertial frame, respectively. Elements $r_{ex}^{(1)}, r_{ey}^{(1)}, r_{ez}^{(1)}, r_{ex}^{(2)}, r_{ey}^{(2)}, r_{ez}^{(2)}$ are the position elements along the $x, y,$ and z axes of the two end-effectors, respectively. Additionally, angles $\phi_1^{(1)}, \phi_2^{(1)}, \phi_3^{(1)}, \phi_1^{(2)}, \phi_2^{(2)}, \phi_3^{(2)}$ represent the rotational angle of each joint of the dual-arm space robot.

According to our earlier work [30], the dynamics of the dual-arm space robot in 3D space can be inferred by the Lagrangian formula used in [32] as

$$A_2\ddot{\phi} + A_1\dot{\phi} = \tau \tag{2}$$

where $A_2 \in \mathbb{R}^{9 \times 9}$ is the coefficient matrix for the second-order term $\ddot{\phi}$, $A_1 \in \mathbb{R}^{9 \times 9}$ is the coefficient matrix for the first-order term $\dot{\phi}$.

In addition, vector $\tau = [\tau_{bx}, \tau_{by}, \tau_{bz}, \tau_1^{(1)}, \tau_2^{(1)}, \tau_3^{(1)}, \tau_1^{(2)}, \tau_2^{(2)}, \tau_3^{(2)}]^T$ stands for the control torques for the base and each joint.

According to the Jacobian equation in (1) and the dynamics in (2), the dynamics of the space robot in the task space can be indicated as

$$\bar{A}_2\ddot{X} + \bar{A}_1\dot{X} = \tau \tag{3}$$

where $\bar{A}_2 = A_2J^{-1} \in \mathbb{R}^{9 \times 9}$ is the coefficient matrix of the second-order term \ddot{X} , and $\bar{A}_1 = A_1J^{-1} - \bar{A}_2\dot{J}J^{-1} \in \mathbb{R}^{9 \times 9}$ is the coefficient matrix of the first-order term \dot{X} . Additionally, $\tau \in \mathbb{R}^9$ is the same control input torque in (2).

A desired variable $X_d \in \mathbb{R}^9$ is defined for vector X of the dual-arm space robot to plan the desired trajectories of the end-effectors. To control the space robot to follow the desired trajectories, an error vector $e = [e_1^T, e_2^T]^T \in \mathbb{R}^{18}$ is defined by

$$e_1 = X - X_d, e_2 = \dot{X} - \dot{X}_d \tag{4}$$

Substituting (3) to the tracking error vector e yields

$$\dot{e}_1 = e_2, \dot{e}_2 = -\bar{A}_2^{-1}\bar{A}_1(e_2 + \dot{X}_d) - \ddot{X}_d + \bar{A}_2^{-1}\tau \tag{5}$$

Then, the control input torques τ can control the dual-arm space robot to track the desired trajectories X_d, \dot{X}_d . In other words, the error vector e converging to zero means the dual-arm space robot follows the desired trajectories to carry out the release operation. Moreover, (5) is used during the approach phase and the postrelease phase.

The space robot and the space object are rigidly connected as a combined system during the pick-up phase. Namely, the dynamics of the combined system can be obtained by the Lagrangian formula used in [32] as

$$\bar{A}'_2\ddot{X} + \bar{A}'_1\dot{X} = \tau \tag{6}$$

where $\bar{A}'_2 \in \mathbb{R}^{9 \times 9}$ and $\bar{A}'_1 \in \mathbb{R}^{9 \times 9}$ are the updated coefficient matrices for the combined system.

During the pick-up phase, the updated tracking errors $e_p = [e_{p1}^T, e_{p2}^T]^T \in \mathbb{R}^{18}$ can be defined as

$$e_{p1} = X - X_d, e_{p2} = \dot{X} - \dot{X}_d \tag{7}$$

The tracking errors of the combined system can be controlled by the control input torques as

$$\dot{e}_{p1} = e_{p2}, \dot{e}_{p2} = -\bar{A}'_2^{-1} \bar{A}'_1 (e_{p2} + \dot{X}_d) - \ddot{X}_d + \bar{A}'_2^{-1} \tau \tag{8}$$

The convergence of the e_p to zero means that the combined system can follow the desired trajectories during the pick-up phase. Also, the desired trajectories will be planned to make the combined system smoothly rotate around the z-axis with respect to the inertial frame at a desired velocity trajectory.

3. Tangent Release Strategy

The attitude and the motion X_d , the velocity \dot{X}_d , and the acceleration \ddot{X}_d need to be planned together for the coordinated control of the base and the manipulators.

The m -th (m is a positive integer)-order Bezier curve [33] is widely used to plan smooth paths. According to the Bezier curve [33], when the order of the Bezier curve is no less than five, we can independently design the attitude and the motion X_d , the velocity \dot{X}_d , and the acceleration \ddot{X}_d . Therefore, we utilize the fifth-order Bezier curve to plan the desired trajectories by

$$\begin{aligned} Y_b(t) = & (1 - \frac{t-t_{b0}}{t_{bf}})^5 P_{b0} + 5(\frac{t-t_{b0}}{t_{bf}})(1 - \frac{t-t_{b0}}{t_{bf}})^4 P_{b1} + \\ & 10(\frac{t-t_{b0}}{t_{bf}})^2 (1 - \frac{t-t_{b0}}{t_{bf}})^3 P_{b2} + 10(\frac{t-t_{b0}}{t_{bf}})^3 (1 - \frac{t-t_{b0}}{t_{bf}})^2 P_{b3} + \\ & 5(\frac{t-t_{b0}}{t_{bf}})^4 (1 - \frac{t-t_{b0}}{t_{bf}}) P_{b4} + (\frac{t-t_{b0}}{t_{bf}})^5 P_{b5}, \quad t_{b0} \leq t \leq t_{bf} \end{aligned} \tag{9}$$

where $Y_b(t)$ represents the trajectory of the fifth-order Bezier curve, point P_{b0} is the start point ($t = t_{b0}$), and P_{b5} is the end point ($t = t_{bf}$) of the 5-th Bezier curve. Points $P_{b1} - P_{b4}$ are the control points.

Based on [30], the smooth desired trajectories X_d during the approach phase ($t \in [t_0, t_a]$) can be desired by the fifth-order Bezier curve in (9) as,

$$\begin{aligned} X_d(t) = & (1 - \frac{t-t_0}{t_a})^5 P_0 + 5(\frac{t-t_0}{t_a})(1 - \frac{t-t_0}{t_a})^4 P_1 + \\ & 10(\frac{t-t_0}{t_a})^2 (1 - \frac{t-t_0}{t_a})^3 P_2 + 10(\frac{t-t_0}{t_a})^3 (1 - \frac{t-t_0}{t_a})^2 P_3 + \\ & 5(\frac{t-t_0}{t_a})^4 (1 - \frac{t-t_0}{t_a}) P_4 + (\frac{t-t_0}{t_a})^5 P_5, \quad t_0 \leq t \leq t_a \end{aligned} \tag{10}$$

When the end-effectors grasp the two handles of the space object, the space robot and the space object will be rigidly connected. Then, the combined system will be controlled to spin around the z-axis of the inertial frame. Since we assume that no external forces or torques to the combined system, the center of mass (CM) is the combine system should be unchanged.

According to [34], we design smooth trajectories for the desired angular velocity $\omega_{cd}(t)$ and the rotational angle vector of the combined system $\theta_{cd}(t)$. During the pick-up phase ($t \in (t_a, t_c]$), the desired value of the rotational angle vector of the combined system θ_{cd} should follow

$$\theta_{cd}(t) = \theta_{cd}(t_a) + (t - t_a)\omega_c(t_a) + (3t_n^5 - t_n^6 - 2.5t_n^4)[\omega_c(t_a) - \omega_c(t_c)](t_c - t_a) \tag{11}$$

where $t \in (t_a, t_c]$ is the current time, and $t_n = (t - t_a)/(t_c - t_a)$. By differentiating the above equation, ω_{cd} can be obtained as

$$\omega_{cd}(t) = \omega_{cd}(t_a) + (15t_n^4 - 6t_n^5 - 10t_n^3)[\omega_c(t_a) - \omega_c(t_c)] \tag{12}$$

Thus, the desired angular velocity of the combined system ω_{cd} can be obtained at the final moment of the capture phase to release the space object. Moreover, the desired trajectories X_d, \dot{X}_d , and \ddot{X}_d can be calculated based on the kinematics of the space robot system.

Finally, the dual-arm space robot smoothly moves back to a stand-by configuration. After releasing by the space robot, the CM of the space object will keep moving at the final linear velocity ($t = t_c$), which can be the tangent velocity of the end-effectors at the moment of t_c . During the postrelease phase ($t \in (t_c, t_p]$), the trajectories of the end-effectors need to be carefully designed to avoid collisions with the space object. Similarly, a smooth fifth high-order Bezier curve in (9) can be developed to plan the desired trajectories of the space robot.

4. Control of the Dual-Arm Space Robot

Sliding Mode Controller

There may be model uncertainties of the space robot and space object. Hence, we assume that there are model uncertainties in the mass and the inertia. A sliding mode controller (SMC) as a robust controller against model uncertainties is selected and developed to carry out the release operation. The control diagram is shown in Figure 3.

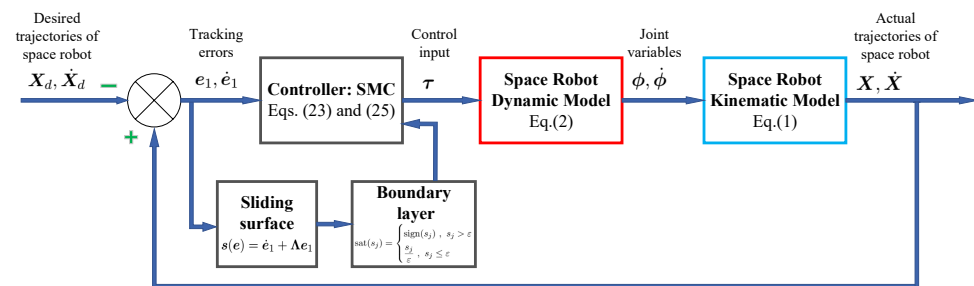


Figure 3. Control diagram for the SMC applied to a dual-arm space robot.

A sliding surface can be expressed as

$$s(e) = \dot{e}_1 + \Lambda e_1 \tag{13}$$

where $\Lambda \in \mathbb{R}^{9 \times 9}$ is a diagonal matrix $\Lambda = \text{diag}([\lambda_1, \lambda_2, \dots, \lambda_9])$, with positive entries λ_j . When the error vector e converges to zero, the state vector X can track the desired trajectories.

By denoting the uncertain term with Δ , the coefficient matrices in (5) with the model uncertainties are denoted as $\hat{A}_2 = \bar{A}_2 + \Delta \bar{A}_2$. The variables with a hat like $\{\hat{\cdot}\}$ define the variables with the model uncertainties.

Unlike the multiple-input multiple-output (MIMO) system in (5), a decoupled system can more easily obtain the independent control gains of the SMC for each channel and tune the gains.

Based on a diagonalization method [35], we decouple the MIMO system in (5) into a set of single-input single-output (SISO) systems as

$$\begin{aligned} \dot{e}_2 &= -\bar{A}_2^{-1} \bar{A}_1 (e_2 + \dot{X}_d) - \ddot{X}_d + \bar{A}_2^{-1} \tau \\ &= -\bar{A}_2^{-1} \bar{A}_1 (e_2 + \dot{X}_d) - \ddot{X}_d + \bar{A}_2^{-1} (\bar{A}_2 + \Delta \bar{A}_2) \tau^* \\ &= f(e, t) + \tau^* + g(e, t) \end{aligned} \tag{14}$$

where $\tau^* = \hat{A}_2^{-1} \tau$ is denoted as the virtual control input torque to the decoupled systems in (14). Also, we define the functions $f(e, t)$ and $g(e, t)$ in (14) as

$$\begin{aligned} f(e, t) &= -\bar{A}_2^{-1} \bar{A}_1(e_2 + \dot{X}_d) - \ddot{X}_d \\ g(e, t) &= \bar{A}_2^{-1} \Delta \bar{A}_2 \tau^* \end{aligned} \tag{15}$$

By assuming the bounded uncertainties applied to the space robot and the object, the coefficient matrices of (14) with the model uncertainties have the following boundary conditions:

$$\begin{cases} \|\bar{A}_2 - \hat{A}_2\| = \|\Delta \bar{A}_2\| \leq \bar{\pi} \|\hat{A}_2\| \\ \bar{a}_1 \|\hat{A}_2\| \leq \|\bar{A}_2\| \leq \bar{a}_2 \|\hat{A}_2\| \\ \bar{b}_1 \|\hat{A}_1\| \leq \|\bar{A}_1\| \leq \bar{b}_2 \|\hat{A}_1\| \\ \bar{c}_1 \|\hat{A}_2^{-1}\| \leq \|\bar{A}_2^{-1}\| \leq \bar{c}_2 \|\hat{A}_2^{-1}\| \end{cases} \tag{16}$$

where $\bar{\pi}, \bar{a}_1, \bar{a}_2, \bar{b}_1, \bar{b}_2, \bar{c}_1, \bar{c}_2$ are positive scalars representing the magnitude of the model uncertainties. Moreover, the difference between the f without the model uncertainties and \hat{f} with the model uncertainties can be obtained as

$$\|f - \hat{f}\| \leq (\bar{b}_2 \bar{c}_2 + 1) \|\hat{A}_2^{-1}\| \|\hat{A}_1\| \|e_2 + \dot{X}_d\| = f^* \tag{17}$$

Similarly, the difference between g and \hat{g} is

$$\|g - \hat{g}\| = \|g\| \leq \bar{c}_2 \bar{\pi} \|\hat{A}_2^{-1}\| \|\hat{A}_2\| \|\hat{A}_2^{-1}\| \tau_{max} = g^* \tag{18}$$

where $\tau_{max} \in \mathbb{R}^9$ stands for the maximum absolute value for the control efforts τ in (5).

For every channel ($j = 1, 2, \dots, 9$), the virtual control effort τ_j^* is to stabilize the errors by

$$\tau_j^* = -\lambda_j e_{2j} - \hat{f}_j - \hat{g}_j - (f_j^* + h_j^* + \alpha_j) \text{sign}(s_j) \tag{19}$$

where α_j is a positive scalar to tune the control gain for the j -th channel of the SMC, and $\text{sign}()$ represents a signum function.

Furthermore, the stability of the SMC can be proved by the Lyapunov method, which indicates that the sliding surface will reach $s(e) = 0$, and the tracking error will converge to zero.

Proof. A positive definite Lyapunov function is selected with $s \neq 0$:

$$V = \frac{1}{2} s^T s \tag{20}$$

Differentiating the Lyapunov function, we obtain the derivative of the Lyapunov function as,

$$\dot{V} = s^T \dot{s} = \sum_{j=1}^9 s_j (\lambda_j e_{2j} + \dot{e}_{2j}) = \sum_{j=1}^9 s_j (\lambda_j e_{2j} + f_j + h_j + \tau_j^*) \tag{21}$$

Then, substituting (19) into \dot{V} yields

$$\begin{aligned} \dot{V} &= \sum_{j=1}^9 s_j [\lambda_j e_{2j} + f_j + g_j - \lambda_j e_{2j} - \hat{f}_j - \hat{g}_j - (f_j^* + g_j^* + \alpha_j) \text{sign}(s_j)] \\ &= \sum_{j=1}^9 [s_j (f_j - \hat{f}_j) + s_j (g_j - \hat{g}_j) - (f_j^* + g_j^* + \alpha_j) |s_j|] \\ &\leq \sum_{j=1}^9 [(|f_j - \hat{f}_j| - f_j^*) |s_j| + (|g_j - \hat{g}_j| - g_j^*) |s_j| - \alpha_j |s_j|] \end{aligned} \tag{22}$$

□

Since (17) and (18) have defined the inequalities, we have $|f_j - \hat{f}_j| - f_j^* \leq 0$ and $|g_j - \hat{g}_j| - g_j^* \leq 0$. Moreover, α_j has been defined as a positive scalar to tune the gain of the SMC. Hence, $\dot{V} \leq 0$. According to the Lyapunov method, the SMC can stabilize the errors in the sliding surface (13).

Since the signum function in (19) may lead to high-frequency switching actions in the SMC, the fluctuations, known as the chattering effect, may exist in the tracking errors and the control input torques. To reduce the fluctuations, we utilize the boundary layer method [28] by

$$\tau_j^* = -\lambda_j e_{2j} - \hat{f}_j - \hat{g}_j - (f_j^* + h_j^* + \alpha_j) \text{sat}(s_j) \tag{23}$$

where function $\text{sat}(s_j)$ is a saturation function defined as

$$\text{sat}(s_j) = \begin{cases} \text{sign}(s_j), & s_j > \varepsilon \\ \frac{s_j}{\varepsilon}, & s_j \leq \varepsilon \end{cases} \tag{24}$$

where ε is a positive scalar to tune the boundary layer thickness. Based on $\tau^* = \hat{A}_2^{-1} \tau$, the control input torque τ of (5) obtained by the SMC can be expressed as

$$\tau = \hat{A}_2 \tau^* \tag{25}$$

Therefore, the SMC is successfully developed to achieve robust control of a dual-arm space robot for a tangent release operation.

5. Numerical Simulation

5.1. Simulation Set-Up

According to the sketch of the tangent release operation plotted in Figure 1, the operation is simulated in three phases: approach phase ($t \in [0, 10]$ s), pick-up phase ($t \in (10, 15]$ s), and postrelease phase ($t \in (15, 30]$ s). The desired angular velocity of the combined system at the release moment when $t = 15$ s is set as $\omega_{cd} = [0, 0, 2]^T$ deg/s. Moreover, we run the following 50 s simulation ($t \in (30, 80]$ s) to make sure the stable status of the space robot. Based on our earlier work [30], the physical data of the dual-arm space robot can be found in Table 1.

Table 1. Physical data for the space robot and the object.

Body	<i>a</i> (m)	<i>b</i> (m)	<i>h</i> (m)	Mass (kg)	Inertia (<i>I_x</i> , <i>I_y</i> , <i>I_z</i>) (kg·m ²)
Base	-	0.5	-	100	(30, 30, 30)
<i>L</i> ₁ ⁽¹⁾	0.25	0.25	-	8	(0.2, 0.0064, 0.2)
<i>L</i> ₂ ⁽¹⁾	0.5	0.5	-	10	(0.008, 0.8, 0.8)
<i>L</i> ₃ ⁽¹⁾	0.5	0.5	-	10	(0.008, 0.8, 0.8)
<i>L</i> ₁ ⁽²⁾	0.25	0.25	-	8	(0.2, 0.0064, 0.2)
<i>L</i> ₂ ⁽²⁾	0.5	0.5	-	10	(0.008, 0.8, 0.8)
<i>L</i> ₃ ⁽²⁾	0.5	0.5	-	10	(0.008, 0.8, 0.8)
RWs	-	-	-	5	(0.3, 0.3, 0.3)
Space object	0.25	0.25	1	42.75	(20, 20, 15)

To avoid singularity configurations of the dual-arm space robot, the initial conditions are carefully set in Table 2.

Table 2. Initial conditions.

Body	Variable	Symbol	Value	Unit
FFSR	Position	${}^a r_g$	$[0, 0, 0]'$	m
	Linear velocity	${}^a v_g$	$[0, 0, 0]'$	m/s
	Angular velocity	${}^a \omega_g$	$[0, 0, 0]'$	rad/s
Base	Attitude	ϕ_s	$[5, 3, 2]'$	°
	Linear velocity	${}^a v_0$	$[0, 0, 0]'$	m/s
	Angular velocity	${}^a \omega_0$	$[0, 0, 0]'$	rad/s
Joint	Angle	$\phi_m^{(1)}$	$[-10, -10, -20]'$	°
	Angle	$\phi_m^{(2)}$	$[-10, -60, 125]'$	°
	Angular velocity	$\dot{\phi}_m^{(1)}$	$[0, 0, 0]'$	rad/s
	Angular velocity	$\dot{\phi}_m^{(2)}$	$[0, 0, 0]'$	rad/s
End-effectors	Position	${}^a r_e^{(1)}$	$[1.6552, 0.4436, 0.2455]'$	m
		${}^a r_e^{(2)}$	$[0.7793, 0.8586, 0.0156]'$	m
Space object frame	Position	${}^a r_{so}$	$[1.1, 0, 0]'$	m
	Angular velocity	${}^t \omega_{so}$	$[0, 0, 0]'$	degree/s
	Linear velocity	${}^a v_{so}$	$[0, 0, 0]'$	m/s
	Attitude	θ_{so}	$[0, 0, 0]'$	°
Grasp points	Position	${}^t r_{soA}$	$[-0.25, 0, 0]'$	m
		${}^t r_{soB}$	$[0.25, 0, 0]'$	m
Combined system	Attitude	${}^a \theta_c$	$[0, 0, 0]'$	°
	Angular velocity	${}^a \omega_c$	$[0, 0, 0]'$	degree/s

5.2. Simulation Results

With the SMC for the coordinated base and motion control of the space robot, numerical simulation results are shown in the following figures. In detail, the control gains for the SMC were tuned as $\lambda_j = 24$, ($j = 1, 2, \dots, 9$), $\alpha_j = 0.01$, $\tau_{maxj} = 1$ Nm, and $\varepsilon = 40$. The parameters for the bounded model uncertainties were set as $\bar{\pi} = 0.3$, $\bar{a}_1 = \bar{b}_1 = \bar{c}_1 = 0.7$, $\bar{a}_2 = \bar{b}_2 = \bar{c}_2 = 1.3$.

For comparison, we select a widely-used computed torque control (CTC) method. Namely, a PD-type CTC was developed for the dual-arm space robot as follows:

$$\tau = \hat{A}_2(\ddot{X}_d - k_v \dot{e}_1 - k_p e_1) + \hat{A}_1 \dot{X} \quad (26)$$

where $k_v = 1$ and $k_p = 2$ were the control gains for the PD controller with the same initial conditions in Table 2. Moreover, we consider the balanced performance of the track accuracy, the magnitude of the control torques, and the smoothness of the tracking errors to tune the control gains.

Figure 4a,b show the errors of the base attitude to the desired attitude by the SMC and the PD controller, respectively. Figure 4c,d show the actual base attitude of the space robot by the SMC and the PD controller, respectively. According to Figure 4a,b, the accuracy of the tracking errors of the base attitude by the SMC (10^{-5} degrees) was higher than by the PD controller (10^{-4} degrees). Therefore, the actual base attitude in Figure 4b,c of the space robot could be controlled to be stable at or near zero during the tangent release operation by the two controllers.

Figure 5a,b show that the tracking accuracy of the EE 1's position is about 10^{-6} m by the SMC and 10^{-5} m by the PD controller, respectively. Thus, the tracking accuracy of the EE1's position by the SMC was higher than that by the PD controller. Figures 5c,d show the actual trajectories of the EE 1 by the two controllers, which describe the smooth motion of the EE 1 to approach, pick-up, release the space object, and finally return to the stable status.

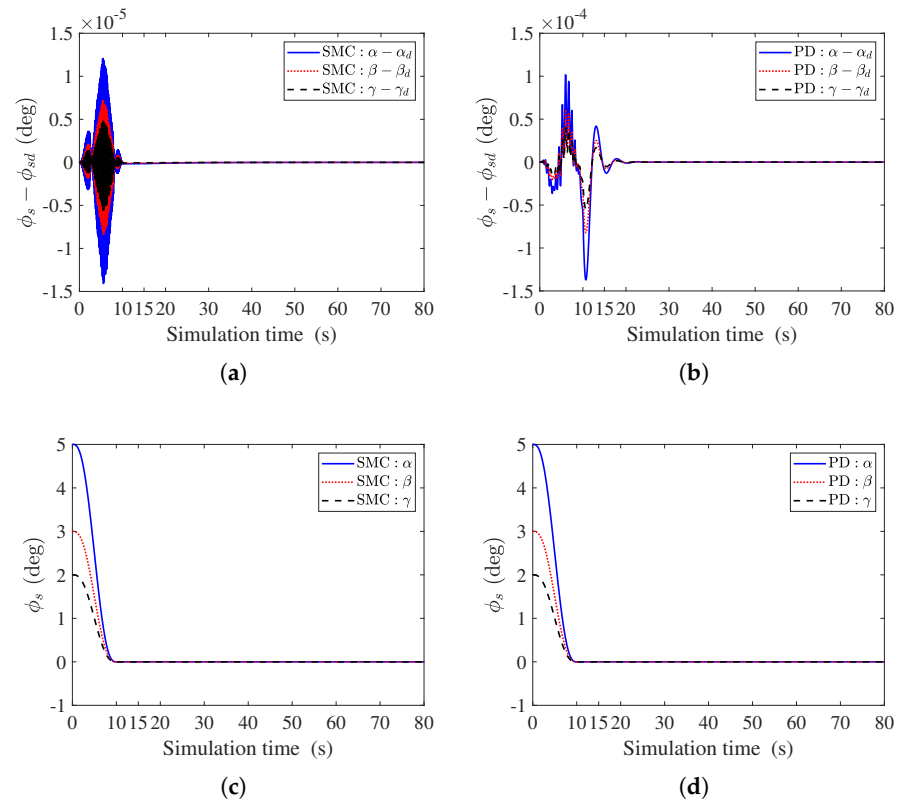


Figure 4. Base attitude performance: (a) tracking errors by SMC; (b) tracking errors by PD; (c) actual trajectories by SMC; (d) actual trajectories by PD.

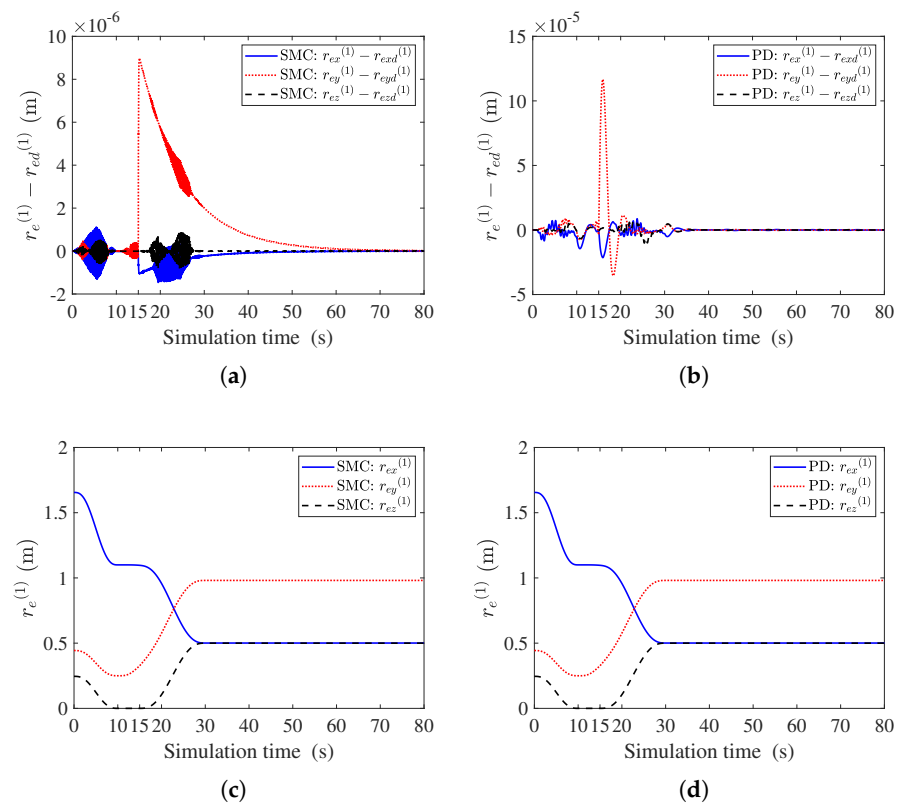


Figure 5. Position of EE 1: (a) tracking errors by SMC; (b) tracking errors by PD; (c) actual trajectories by SMC; (d) actual trajectories by PD.

Similarly, Figure 6a,b show the tracking accuracy of the EE 2's position is about 10^{-6} m by the SMC and 10^{-5} m by the PD controller, respectively. Figure 6c,d shows the actual trajectories of the EE 2, which demonstrate good cooperation of the two end-effectors by the two controllers. Also, the SMC had better performance than the PD controller.

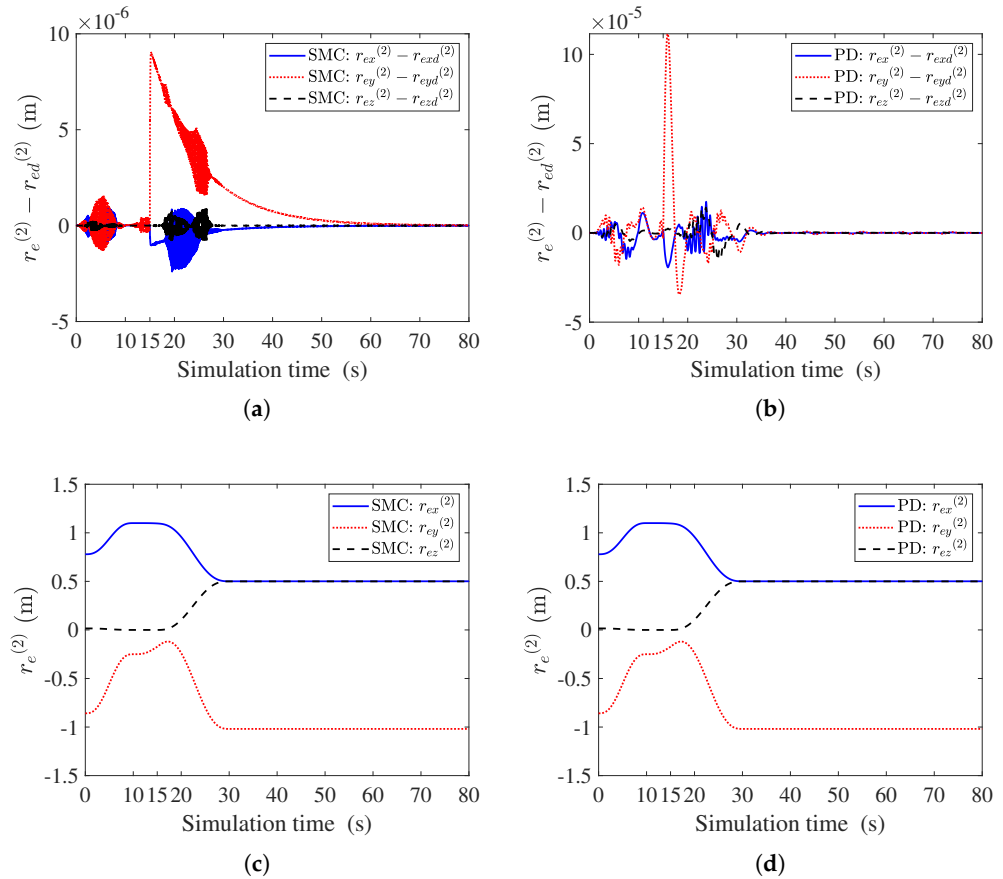


Figure 6. Position of EE 2: (a) tracking errors by SMC; (b) tracking errors by PD; (c) actual trajectories by SMC; (d) actual trajectories by PD.

Figure 7 demonstrates the control input torques for the base attitude, Arm 1, and Arm 2, by the SMC and the PD controller, respectively. According to Figure 7, the SMC and the PD controller can deliver the similar control input torques with smoothness and feasibility for the tangent release operation.

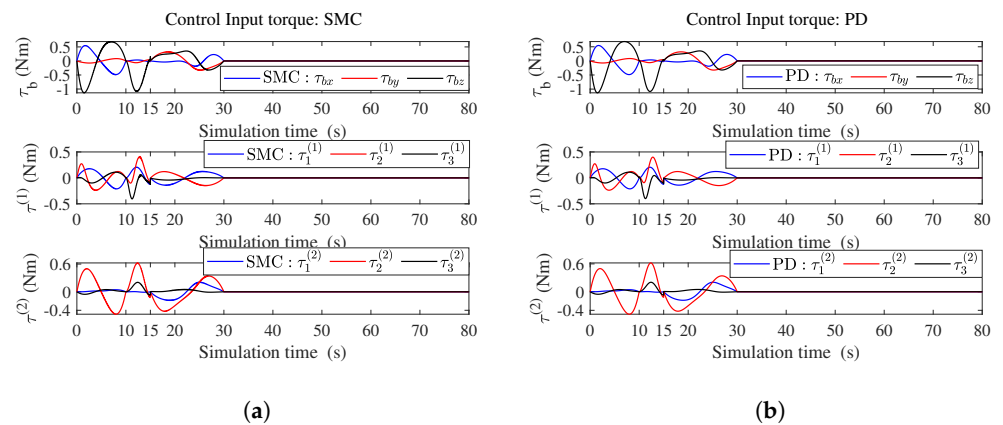


Figure 7. Control input torques: (a) control torques by SMC; (b) control torques by PD.

Figure 8 shows the position vector and the velocity vector of the CM of the space object during the tangent release operation by the two controllers with similar results. The CM of the space object was stationary during the approach phase ($t \in [0, 10]$ s), captured and accelerated during the pick-up phase ($t \in (10, 15]$ s), and released at the moment ($t = 15$ s). Then, the space object kept moving at the desired released velocity, and the space robot moved back to a safe stand-by configuration during the postrelease phase ($t \in (15, 30]$ s).

Figure 9 demonstrates the angular velocity of the combined system including the space robot and the object during the pick-up phase by the two controllers with similar results. According to Figure 9, the angular velocity of the combined system was smoothly accelerated to the desired value $\omega_{cd} = [0, 0, 2]^T$ deg/s at the releasing moment $t = 15$ s.

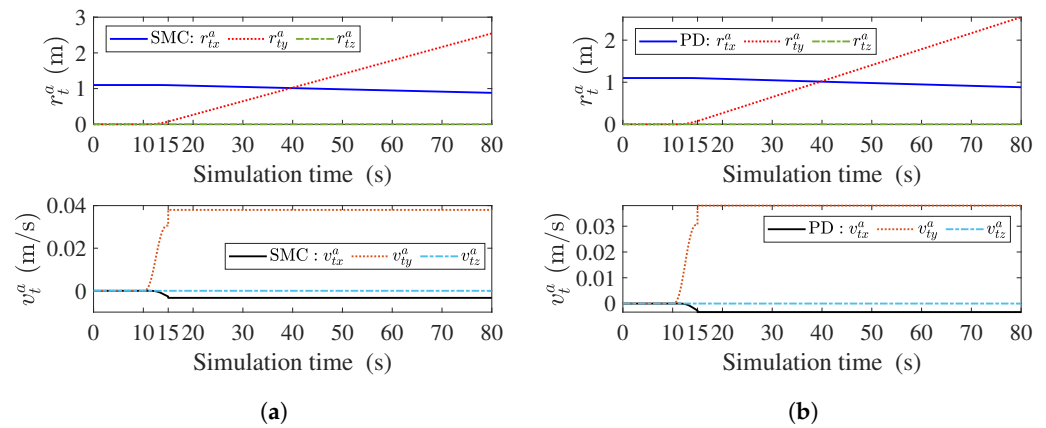


Figure 8. The CM of space object’s position and velocity: (a) by SMC; (b) by PD.

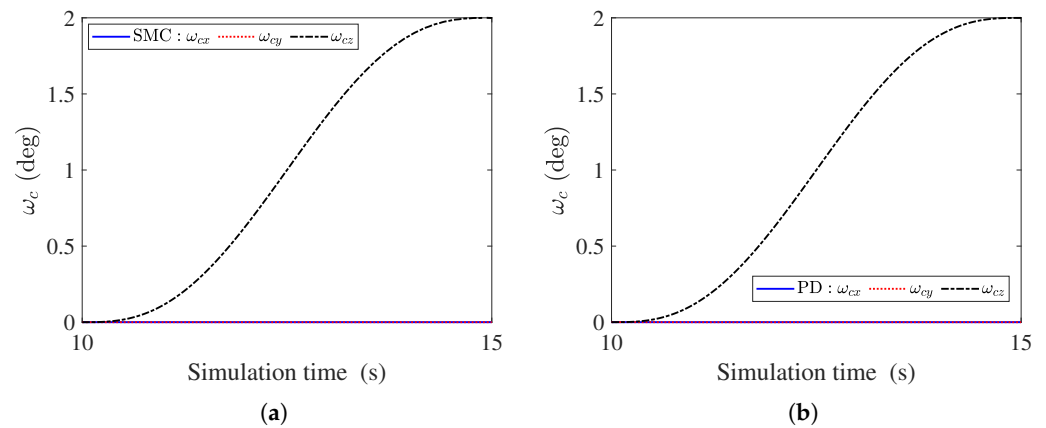


Figure 9. The angular velocity of the combined system: (a) by SMC; (b) by PD.

5.3. Robustness against Model Uncertainties

To compare the robustness against the model uncertainties by the controllers, a set of uncertain parameters are applied to the space robot system. By introducing a scalar κ , the magnitude of the model uncertainties for the mass and moment of inertia of the space robot and space object is shown by

$$m_i^{(k)} = \kappa \hat{m}_i^{(k)} \quad (i = 1, 2, 3, k = 1, 2), \quad I_i^{(k)} = \kappa \hat{I}_i^{(k)}, \quad m_t = \kappa \hat{m}_{s0}, \quad I_t = \kappa \hat{I}_{s0} \quad (27)$$

where $\hat{m}_i^{(k)}$, $\hat{I}_i^{(k)}$, \hat{m}_{s0} , and \hat{I}_{s0} are the values of the mass and inertia with the model uncertainties, respectively. Different values of κ represent the different magnitudes of the model uncertainties. Additionally, $\kappa = 1$ means no model uncertainties are applied to the space robot and the space object.

Figure 10a,b plot the box charts for the tracking errors of the base attitude by the SMC and the PD controller, respectively. Figure 10c,d show the box charts for the tracking errors of the position of the end-effectors by the SMC and the PD controller, respectively. The box charts can show the range and the distribution of the tracking errors. According to Figure 10, the errors can be larger when the magnitude of the uncertainties ($\pm 10\%$, $\pm 20\%$) was more extensive. In addition, the SMC had better robustness against the model uncertainties than the PD controller because more minor tracking errors could be found while the model uncertainties were applied.

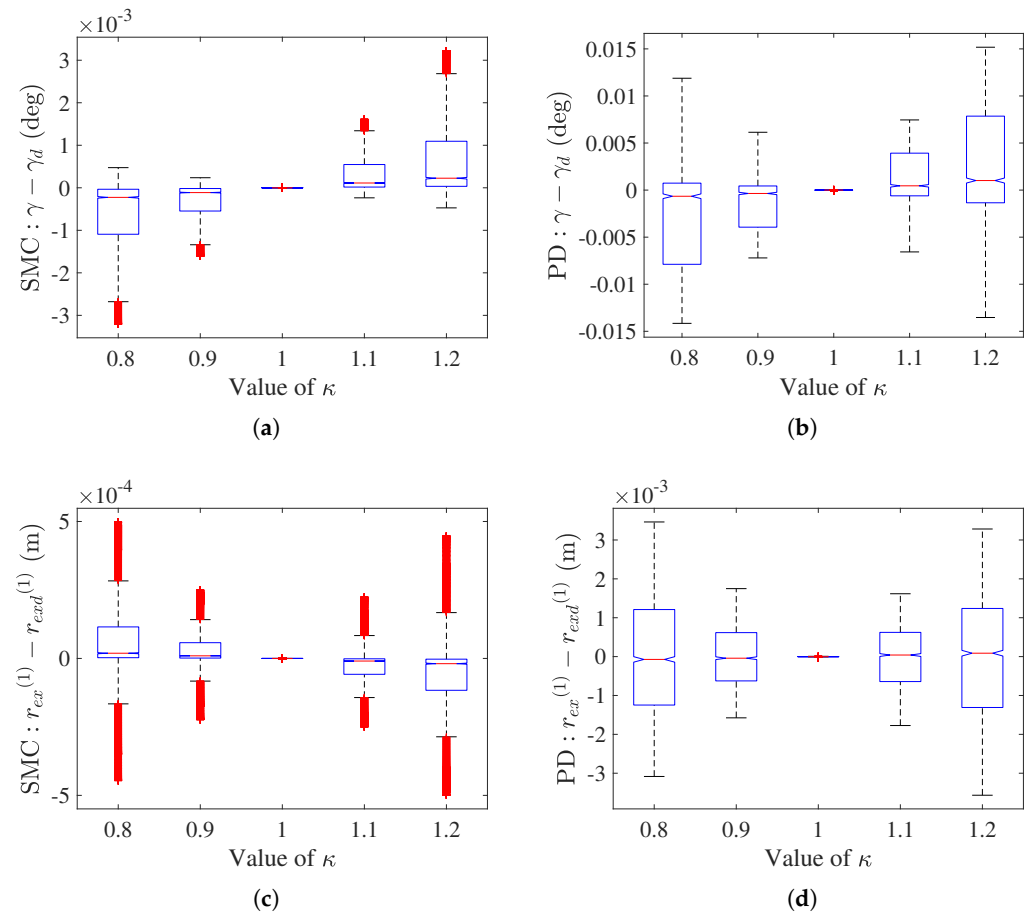


Figure 10. Robust performance against the model uncertainties: (a) errors' range of base attitude by SMC; (b) errors' range of base attitude by PD; (c) errors' range of EEs' position by SMC; (d) errors' range of EEs' position by PD.

6. Conclusions

This paper addresses a new proposal to tangentially release a space object by a dual-arm space robot. This tangent release strategy can make a free-floating space robot transport a space object like cargo in space at a desired tangent velocity without the need for thrusters and the associated fuel consumption. Unlike pushing the space object away, the releasing directions can be variable to satisfy the requirements of complex on-orbit space missions. For an explanation of the strategy, the two end-effectors can approach and pick up a payload from the cargo bay for deployment, then release the object in a tangent direction to a desired destination. Then, the robot and the object are rigidly connected as a combined system. When the combined system reaches the desired velocity, the space robot will release the space object along its tangent direction. After the release maneuver, the space robot will follow a planned safe and smooth trajectory to a stationary configuration. Meanwhile, the space object will keep the tangent velocity at the releasing moment, which can be used for cargo transportation in the neighborhood. The base attitude can be controlled at or near

zero when the coupled dynamics of the space robot exist. Considering uncertain inertial parameters applied to the space robot and the object, robust controllers help control the space robot. A robust sliding mode controller (SMC) is developed to control the space robot with good robustness and high tracking accuracy. Moreover, a conventional PD-type computed torque controller (CTC) is chosen for comparison. According to the simulation results, the SMC presented smaller tracking errors and better robustness against the model uncertainties than the PD controller.

Although we utilize the boundary layer method to reduce the fluctuations caused by SMC, there are vibrations in the tracking errors for the desired trajectories of the space robot. In the future, we will develop advanced control methods to improve the smoothness of tracking errors. Moreover, limitations of our proposed tangent strategy are related to external disturbances like mechanical vibrations caused by physical contact with the space object, which will be further investigated in our future work.

Author Contributions: Conceptualization X.W. and J.K.; methodology, X.W.; software, X.W.; validation, X.W.; formal analysis, X.W.; investigation, X.W. and J.K.; resources, X.W. and J.K.; data curation, X.W.; writing—original draft preparation, X.W.; writing—review and editing, J.K.; visualization, X.W.; supervision, J.K.; project administration, X.W. and J.K.; funding acquisition, not available. All authors have read and agreed to the published version of the manuscript.

Funding: This research received no external funding.

Institutional Review Board Statement: Not applicable.

Informed Consent Statement: Not applicable.

Data Availability Statement: The data presented in this article are available on reasonable request from the authors.

Conflicts of Interest: The authors declare that they have no known competing financial interests or personal relationships that could have appeared to influence the work reported in this paper.

References

1. Moosavian, S.A.A.; Papadopoulos, E. Free-flying robots in space: An overview of dynamics modeling, planning and control. *Robotica* **2007**, *25*, 537–547. [[CrossRef](#)]
2. Flores-Abad, A.; Ma, O.; Pham, K.; Ulrich, S. A review of space robotics technologies for on-orbit servicing. *Prog. Aerosp. Sci.* **2014**, *68*, 1–26. [[CrossRef](#)]
3. Shi, L.; Yao, H.; Shan, M.; Gao, Q.; Jin, X. Robust control of a space robot based on an optimized adaptive variable structure control method. *Aerosp. Sci. Technol.* **2022**, *120*, 107267. [[CrossRef](#)]
4. Ouyang, X.; Meng, D.; Wang, X.; Wang, C.; Liang, B.; Ding, N. Hybrid rigid-continuum dual-arm space robots: Modeling, coupling analysis, and coordinated motion planning. *Aerosp. Sci. Technol.* **2021**, *116*, 106861. [[CrossRef](#)]
5. Guo, J.; Zhao, Y.; Xu, Y.; Zhang, G.; Yao, J. A novel modular deployable mechanism for the truss antenna: Assembly principle and performance analysis. *Aerosp. Sci. Technol.* **2020**, *105*, 105976. [[CrossRef](#)]
6. Jin, R.; Rocco, P.; Geng, Y. Cartesian trajectory planning of space robots using a multi-objective optimization. *Aerosp. Sci. Technol.* **2021**, *108*, 106360. [[CrossRef](#)]
7. Huang, Z.; Chen, G.; Shen, Y.; Wang, R.; Liu, C.; Zhang, L. An Obstacle-Avoidance Motion Planning Method for Redundant Space Robot via Reinforcement Learning. *Actuators* **2023**, *12*, 69. [[CrossRef](#)]
8. Syromiatnikov, V.S. Manipulator system for module re docking on the Mir Orbital Complex. In Proceedings of the 1992 IEEE International Conference on Robotics and Automation. IEEE Computer Society, Nice, France, 12–14 May 1992; pp. 913–914.
9. Yoshida, K.; Kurazume, R.; Umetani, Y. Dual arm coordination in space free-flying robot. In Proceedings of the ICRA, Citeseer, Sacramento, CA, USA, 9–11 April 1991; pp. 2516–2521.
10. Control system for free-floating space manipulator based on nonlinear model predictive control (NMPC). *J. Intell. Robot. Syst.* **2017**, *85*, 491–509. [[CrossRef](#)]
11. Yang, S.; Wen, H.; Hu, Y.; Jin, D. Coordinated motion control of a dual-arm space robot for assembling modular parts. *Acta Astronaut.* **2020**, *177*, 627–638. [[CrossRef](#)]
12. Xu, W.; Meng, D.; Liu, H.; Wang, X.; Liang, B. Singularity-free trajectory planning of free-floating multiarm space robots for keeping the base inertially stabilized. *IEEE Trans. Syst. Man Cybern. Syst.* **2017**, *49*, 2464–2477. [[CrossRef](#)]
13. Raina, D.; Shah, S.V. Impact modeling and estimation for multi-arm space robot while capturing tumbling orbiting objects. In Proceedings of the Advances in Robotics, New Delhi, India, 28 June–2 July 2017; pp. 1–6.

14. Peng, J.; Xu, W.; Wang, Z.; She, Y. Dynamic analysis of the compounded system formed by dual-arm space robot and the captured target. In Proceedings of the 2013 IEEE International Conference on Robotics and Biomimetics (ROBIO), Shenzhen, China, 12–14 December 2013; pp. 1532–1537.
15. Liu, E.; Yang, Y.; Yan, Y. Spacecraft attitude tracking for space debris removal using adaptive fuzzy sliding mode control. *Aerosp. Sci. Technol.* **2020**, *107*, 106310. [[CrossRef](#)]
16. Shi, L.; Kayastha, S.; Katupitiya, J. Robust coordinated control of a dual-arm space robot. *Acta Astronaut.* **2017**, *138*, 475–489. [[CrossRef](#)]
17. Wang, X.; Shi, L.; Katupitiya, J. Robust control of a dual-arm space robot for in-orbit screw-driving operation. *Acta Astronaut.* **2022**, *200*, 139–148. [[CrossRef](#)]
18. Jia, Y.; Misra, A.K. Robust trajectory tracking control of a dual-arm space robot actuated by control moment gyroscopes. *Acta Astronaut.* **2017**, *137*, 287–301. [[CrossRef](#)]
19. Jia, Y.H.; Hu, Q.; Xu, S.J. Dynamics and adaptive control of a dual-arm space robot with closed-loop constraints and uncertain inertial parameters. *Acta Mech. Sin.* **2014**, *30*, 112–124. [[CrossRef](#)]
20. Yan, L.; Xu, W.; Hu, Z.; Liang, B. Multi-objective configuration optimization for coordinated capture of dual-arm space robot. *Acta Astronaut.* **2020**, *167*, 189–200. [[CrossRef](#)]
21. Mohamed, A.; Saaj, C.; Seddaoui, A.; Eckersley, S. Controlling a non-linear space robot using linear controllers. In Proceedings of the 5th CEAS Conference on Guidance, Navigation and Control (EuroGNC), Milan, Italy, 3–5 April 2019; CEAS: Milan, Italy, 2019.
22. Moradi, M. Self-tuning PID controller to three-axis stabilization of a satellite with unknown parameters. *Int. J. Non-Linear Mech.* **2013**, *49*, 50–56. [[CrossRef](#)]
23. Tang, Z.; He, S.; Yang, M.; Pei, Z. Adaptive control based on neural network for uncertain space robot. In Proceedings of the 2011 International Conference on Photonics, 3D-Imaging, and Visualization. International Society for Optics and Photonics, Guangzhou, China, 16–19 May 2011; Volume 8205, p. 82052Z.
24. Zubov, N.; Lapin, A.; Ryabchenko, V.; Proletarsky, A.; Selezneva, M.; Neusypin, K. A Robust Control Algorithm of a Descent Vehicle Angular Motion in the Earth's Atmosphere. *Appl. Sci.* **2022**, *12*, 731. [[CrossRef](#)]
25. He, G.; Cao, D. Dynamic Modeling and Attitude–Vibration Cooperative Control for a Large-Scale Flexible Spacecraft. *Actuators* **2023**, *12*, 167. [[CrossRef](#)]
26. Zhang, X.; Liu, J.; Gao, Q.; Ju, Z. Adaptive robust decoupling control of multi-arm space robots using time-delay estimation technique. *Nonlinear Dyn.* **2020**, *100*, 2449–2467. [[CrossRef](#)]
27. Feng, C.; Chen, W.; Shao, M.; Ni, S. Trajectory Tracking and Adaptive Fuzzy Vibration Control of Multilink Space Manipulators with Experimental Validation. *Actuators* **2023**, *12*, 138. [[CrossRef](#)]
28. Slotine, J.J.E. The robust control of robot manipulators. *Int. J. Robot. Res.* **1985**, *4*, 49–64. [[CrossRef](#)]
29. Wang, X.; Shi, L.; Katupitiya, J. A strategy to decelerate and capture a spinning object by a dual-arm space robot. *Aerosp. Sci. Technol.* **2021**, *113*, 106682. [[CrossRef](#)]
30. Wang, X.; Shi, L.; Katupitiya, J. Coordinated Control of a Dual-arm Space Robot to Approach and Synchronise with the Motion of a Spinning Target in 3D Space. *Acta Astronaut.* **2020**, *176*, 99–110. [[CrossRef](#)]
31. Shi, L.; Xiao, X.; Shan, M.; Wang, X. Force control of a space robot in on-orbit servicing operations. *Acta Astronaut.* **2022**, *193*, 469–482. [[CrossRef](#)]
32. Hollerbach, J.M. A recursive lagrangian formulation of manipulator dynamics and a comparative study of dynamics formulation complexity. *IEEE Trans. Syst. Man Cybern.* **1980**, *10*, 730–736. [[CrossRef](#)]
33. Bézier, P.E. *How Renault Uses Numerical Control for Car Body Design and Tooling*; Technical Report, SAE Technical Paper; SAE International: Warrendale, PA, USA, 1968.
34. Yamawaki, T.; Yashima, M. Arm trajectory planning by controlling the direction of end-point position error caused by disturbance. In Proceedings of the 2008 IEEE/ASME International Conference on Advanced Intelligent Mechatronics, Xian, China, 2–5 July 2008; pp. 1120–1125.
35. DeCarlo, R.A.; Zak, S.H.; Matthews, G.P. Variable structure control of nonlinear multivariable systems: A tutorial. *Proc. IEEE* **1988**, *76*, 212–232. [[CrossRef](#)]

Disclaimer/Publisher's Note: The statements, opinions and data contained in all publications are solely those of the individual author(s) and contributor(s) and not of MDPI and/or the editor(s). MDPI and/or the editor(s) disclaim responsibility for any injury to people or property resulting from any ideas, methods, instructions or products referred to in the content.